CHEMISTRY
A European Journal

A Journal of
ChemPubSoc Europe

Accepted Article

Title: Dynamic Motion of Organic Ligands in Polar Layered Cobalt Phosphonates

Authors: Zhong-Sheng Cai, Norihisa Hoshino, Song-Song Bao, Jiage Jia, Tomoyuki Akutagawa, and Li-Min Zheng

To be cited as: *Chem. Eur. J.* 10.1002/chem.201801301

Link to VoR: http://dx.doi.org/10.1002/chem.201801301

Supported by
ACES

WILEY-VCH

Dynamic Motion of Organic Ligands in Polar Layered Cobalt Phosphonates

Zhong-Sheng Cai,[a] Norihisa Hoshino,[b] Song-Song Bao,[a] Jiage Jia,[a] Tomoyuki Akutagawa,*[b] and Li-Min Zheng*[a]

Abstract: By introducing polar methoxy group into phenyl- or benzyl-phosphonate ligands, four cobalt phosphonates with layered structures are obtained, namely, Co(4-mopp)(H_2O) (**1**), Co(4-mobp)(H_2O) (**2**), Co(3-mopp)(H_2O) (**3**) and Co(3-mobp)(H_2O) (**4**), where 4- or 3-moppH_2 is (4- or 3-methoxyphenyl)phosphonic acid and 4- or 3-mobpH_2 is (4- or 3-methoxybenzyl)phosphonic acid. Compounds **1**, **2** and **4** crystallize in polar space groups $Pmn2_1$ or $Pna2_1$, while compound **3** crystallizes in a centrosymmetric space group $P2_1/n$. The layer topologies in the four structures are similar and can be viewed as perovskite-type, where the edge-sharing [Co_4O_4] rhombuses are capped by the PO_3C groups. The phenyl and Me-O groups in compounds **1**-**3** are heavily disordered, while that in **4** is ordered. Structural comparison based on the data at 296 K and 123 K reveals distinct dynamic motion of the organic groups in compounds **1** and **2**. The fluctuation of polar Me-O groups in these two compounds is confirmed by the dielectric relaxation measurements. In contrast, the fluctuation of polar groups in compounds **3** and **4** is not evident. Interestingly, the dehydrated samples of **3** and **4** (**3-de** and **4-de**) exhibit one-step and two-step phase transitions associated with the motion of polar organic groups, as proved by the DSC and dielectric measurements. Magnetic properties of compounds **1-4** are investigated, and strong antiferromagnetic interactions are found to mediate between the magnetic centers through μ-O(P) and O-P-O bridges.

Introduction

Studies on the dynamic motions in crystalline solids have been a challenging but very interesting task for the development of molecular machines and devices.[1-3] While most of the work have been focused on the discrete molecules, for example molecular gyroscopes,[4-8] much less has been explored for materials with extended network structures.[1,9,10]

Metal-organic frameworks which show precise structures that can be designed and constructed through judicious choice of metal ions and ligands offer an unprecedented structural and chemical diversity. A number of new architectures with various pore sizes, shapes and chemical functions have been obtained, which show promising potential applications in gas storage and separation,[11-14] catalysis,[15,16] proton conduction[17,18] and magnetism[19] etc. MOFs can also be good candidates for studying the molecular motor dynamics because of their porosity, thermal stability and flexibility, which allow the free rotation of organic ligands.[20-26] However, the rotation frequency of the ligands can be affected or controlled by the structures such as the shape and volume of the pores, temperature and other external stimulus. In some cases, temperature dependent order-disorder transition occurs for the polar rotation components leading to interesting dielectric or ferroelectric properties.[27-30] Further, when a paramagnetic metal ion is introduced to the system, multifunctional materials can be obtained.[31-33] Nevertheless, dynamic motion on non-porous layered MOF materials has rarely been documented.[34-36]

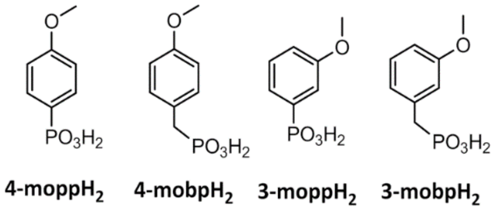

Scheme 1. The chemical structures of the ligands.

Metal phosphonates are an important class of organic-inorganic hybrid materials showing versatile structures and intriguing functions.[37,38] Most of them were reported to exhibit layered or pillared layered structures in which the inorganic layers of M-PO_3 with different topologies are separated by the organic components. The layered inorganic backbone can provide rigid frames to serve as the stator, and the organic part can undergo rotation between the layers. Thus layered or pillared layered metal phosphonates can provide good candidates for constructing amphidynamic crystals. Surprisingly, however, dynamic motions of organic ligands in metal phosphonate systems have never been described thus far, partly because of their dense and

---

[a] Dr. Z.-S. Cai, Prof. Dr. S.-S. Bao, Jiage Jia, Prof. Dr. L.-M. Zheng
State Key Laboratory of Coordination Chemistry, School of Chemistry and Chemical Engineering, Collaborative Innovation Center of Advanced Microstructures
Nanjing University
Nanjing 210023, P. R. China
E-mail: lmzheng@nju.edu.cn
http://hysz.nju.edu.cn/lmzheng/
[b] Dr. Norihisa Hoshino, Prof. Dr. Tomoyuki Akutagawa
Institute of Multidisciplinary Research for Advanced Materials (IMRAM), Tohoku University,
Sendai 980-8577, Japan
E-mail: akuta@tagen.tohoku.ac.jp

Supporting information for this article is given via a link at the end of the document.

Table 1. Crystallographic data for compounds **1-4** at 296 K.

Compound	**1**	**2**	**3**	**4**
Formula	$C_7H_9CoO_5P$	$C_8H_{11}CoO_5P$	$C_7H_9CoO_5P$	$C_8H_{11}CoO_5P$
M	263.04	277.07	263.04	277.07
crystal system	orthorhombic	orthorhombic	monoclinic	orthorhombic
space group	$Pmn2_1$ (No. 31)	$Pmn2_1$ (No. 31)	$P2_1/n$ (No. 14)	$Pna2_1$ (No. 33)
a / Å	5.6146(8)	5.7121(6)	4.8553(4)	35.022(3)
b / Å	17.656(3)	17.8425(19)	32.281(2)	4.8180(5)
c / Å	4.8382(7)	4.8150(5)	5.6773(4)	5.7163(5)
β / °	90	90	91.788(1)	90
V / Å^3, Z	479.62(13), 2	490.74(9), 2	889.39(11), 4	964.55(15), 4
D_c / g cm^{-3}	1.820	1.875	1.964	1.908
F(000)	266	282	532	564
GoF on F^2	1.000	1.001	1.007	0.970
R_1, wR_2[a] [$I>2\sigma(I)$]	0.0289, 0.0661	0.0466, 0.0866	0.0339, 0.0658	0.0487, 0.1196
(all data)	0.0315, 0.0672	0.0640, 0.0956	0.0559, 0.0721	0.0632, 0.1313
$(\Delta\rho)_{\max,\min}$ / e Å^{-3}	0.54, -0.60	0.118, -0.875	0.446, -0.405	0.883, -0.576
CCDC number	1828984	1828986	1529373	1828990

$^aR_1 = \Sigma||F_o| - |F_c||/\Sigma|F_o|$, $wR_2 = [\Sigma w(F_o^2 - F_c^2)^2/\Sigma w(F_o^2)^2]^{1/2}$

Table 2. The Co-O and Co···Co distances (Å) and O-Co-O and Co-O-Co angles (°) in structures **1-4** at 296 K.

Compound	Co-O	O-Co-O	Co···Co[a]	∠Co-O-Co
1	2.059(1) - 2.229(1)	66.8(1) - 175.7(2)	3.729(1)	120.6(1)
2	2.056(5) - 2.226(5)	66.5(2) - 174.8(3))	3.759(1)	122.7(1)
3	2.055(2) - 2.278(2)	66.3(1) - 174.1(1)	3.701(1), 3.815(1)	119.6(1), 122.0(1)
4	2.049(5) - 2.267(5)	66.7(2) - 173.3(2)	3.760(1)	121.1(1), 123.9(1)

[a] The Co···Co distance over μ-O bridge

nonporous nature and the presence of inter-molecular interactions which block the free motion of the organic moieties within the structure. To promote the rotation frequency of the organic groups in metal aromatic phosphonates, the introduction of a proper substituent into the aromatic rings can be a useful strategy to weaken the inter-molecular interactions such as π-π interactions. In particular, when the substituent is polar, dielectric or even ferroelectric properties associated with order-disorder phase transitions could be observed. Following this train of thought, we designed and synthesized four aromatic phosphonate ligands containing para- or meta-substituted polar Me-O group, namely, (4- or 3-methoxyphenyl)phosphonic acid [4- or 3-moppH$_2$] and (4- or 3-methoxybenzyl)phosphonic acid [4- or 3-mobpH$_2$] (Scheme 1). The latter two are more flexible due to the presence of an additional methyl group.

In this paper, we report four cobalt phosphonates based on these phosphonate ligands, formulated as Co(4-mopp)(H_2O) (**1**), Co(4-mobp)(H_2O) (**2**), Co(3-mopp)(H_2O) (**3**) and Co(3-mobp)(H_2O) (**4**). Single crystal structural determinations reveal that compounds **1**, **2** and **4** are polar. While compound **3** is non-polar, the structure of which has already been described in a recent work.[39] All four compounds display similar layered structures with the layer topology of perovskite-type. The organic groups in compounds **1-3** are heavily disordered at both 296 K and 123 K, but those in **4** are well ordered even at 296 K. The anisotropic parameter analysis reveals distinct fluctuation of the Ph-OMe groups in the para-substituted compounds **1** and **2**, also supported by dielectric measurements. More interestingly, the dehydrated samples **3-de** and **4-de** show temperature dependent dielectric anomalies related to phase transitions. Finally, the magnetic properties of **1-4** are studied, and dominant antiferromagnetic interactions are found in all compounds.

Results and Discussion

Description of structures 1-4

Single crystal structures of compounds **1-4** were measured at 296 K. Although structure **3** at room temperature was already reported, the crystallographic data and selected structural parameters of all four compounds are given for a comparison (Tables 1 and 2). It is clear that three of the four structures (**1**, **2**, **4**) are polar, while compound **3** is centrosymmetric.

Compound **1** crystallizes in the polar space group $Pmn2_1$ (No. 31). Its asymmetric unit consists of one Co^{II}, one 4-mopp^{2-} and one coordinated water molecule (Figure S3). The Co1 atom has a distorted octahedral geometry surrounded by six oxygen atoms, five from phosphonate ligands (O1A, O1B, O1C, O1D and O2) and one from water molecule (O1W). The Co-O bond lengths fall in the range of 2.059(1) - 2.229(1) Å. The 4-mopp^{2-} serves as a penta-dentate ligand, two of its three phosphonate oxygen atoms act as μ-O bridges to connect the Co^{II} ions. An inorganic layer structure is thus constructed which contains edge-sharing [Co_4O_4]

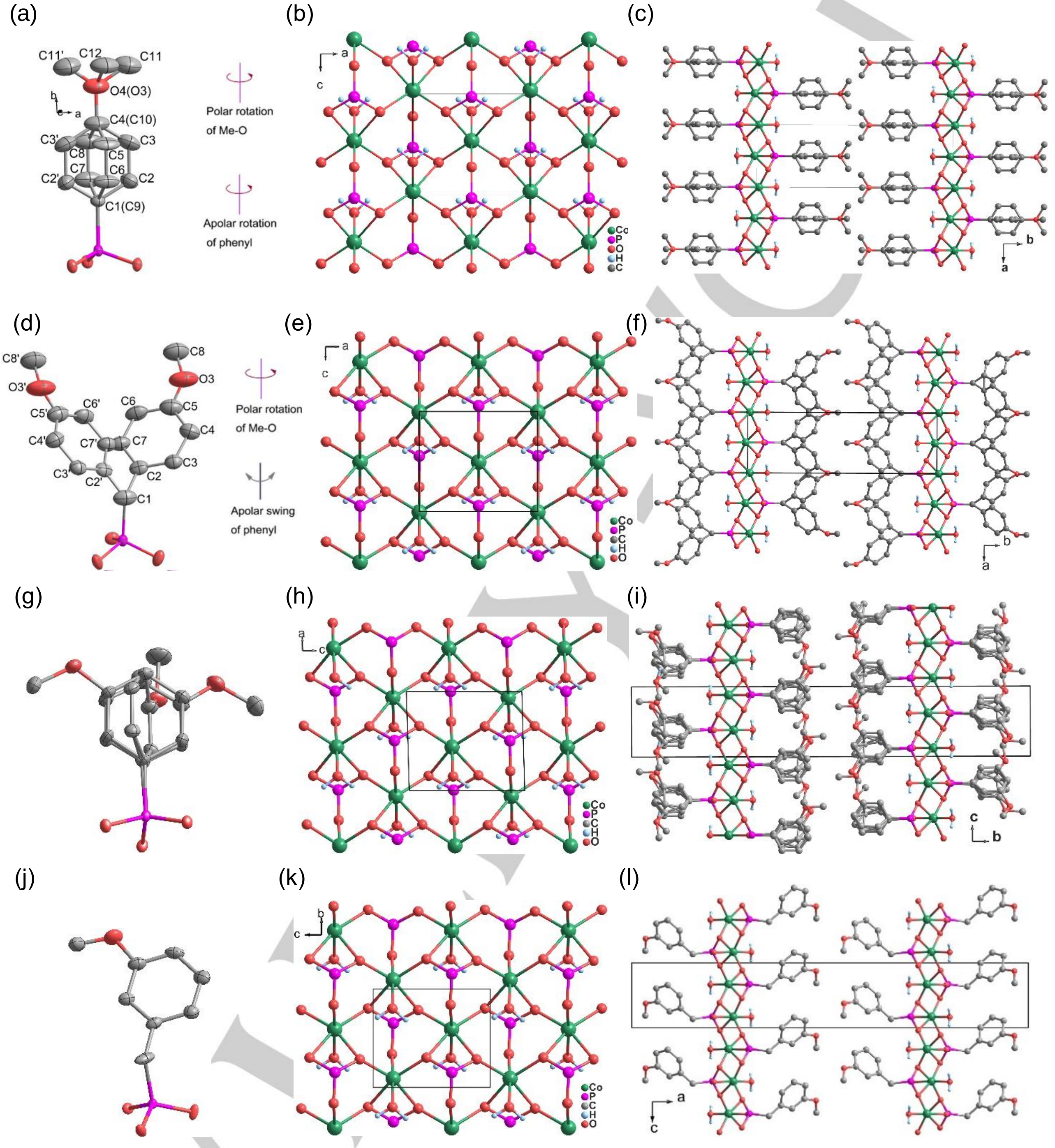

Figure 1. Structures of compounds **1** (a, b, c), **2** (d, e, f), **3** (g, h, i) and **4** (j, k, l). Ellipsoid representation of the ligands showing the motion of the disordered atoms and phenyl groups (a, d, g, j), single inorganic layers in the *ac* or *bc* plane (b, e, h, k) and packing diagrams viewed along the *c*-axis (c, f) or *a*-axis (i) or *b*-axis (l).

rhombus (Figure 1). Within the rhombus, the Co···Co distance over μ-O is 3.729(1) Å and the Co-O-Co angle is 120.6(1)°. The layer is not flat, but slightly undulated along the *b*-axis. The PO_3C groups are capped on the rhombus with the organic tails filling in the interlayer space (Figure 1c). The layer topology can be approximately described as a perovskite-type, similar to those of $M(PhPO_3)(H_2O)$ (M = Mg, Zn, Mn, Ca, Cd).[40, 41] Notably, the neighboring phosphonate ligands are apart from each other by 4.838(1) Å such that π-π interactions are not present in the structure. The phenyl and Me-O groups are disordered over two sites (Figure 1a). Van der Waals interactions are dominant between the layers.

The structure of compound **2** is similar to that of **1** except that the benzyl group replaces the phenyl group in **1** (Figure 1d). It also crystallizes in the polar space group $Pmn2_1$, and shows a layer structure containing edge-sharing [Co$_4$O$_4$] rhombus. Compared with those in **1**, the Co⋯Co distance over the μ-O bridge [3.759(1) Å] and the Co-O-Co angle [122.7(1)°] are slightly larger, while the adjacent P⋯P distance [4.815(1) Å] is slightly shortened. More significant difference is that the Ph-OMe group as a whole are disordered over two sites in **2**, unlike compound **1** in which the phenyl and Me-O groups are disordered individually (Figure 1).

When meta-substituted Me-O groups are introduced into the pheny or benzyl phosphonate ligands, compounds **3** and **4** are obtained. Although both show analogous layer structures, compound **4** crystallizes in a polar space group $Pna2_1$ (No. 33), while **3** crystallizes in a centrosymmetric space group $P2_1/n$. In these two cases, the [Co$_4$O$_4$] rhombus becomes slightly distorted. For **3**, the Co⋯Co distances are 3.701(1) and 3.815(1) Å and the Co-O-Co angles are 119.6(1) and 122.0(1)°. For **4**, the edge distance is the same [Co⋯Co: 3.760(1) Å] but the Co-O-Co angles are 121.1(1) and 123.9(1)°. The dangling Ph-OMe groups are disordered over three different sites in **3**, but completely ordered in **4** (Figure 1).

Comparison of anisotropic parameters of 1-3 at 296 K and 123 K

Considering that the organic groups of the phosphonate ligands in compounds **1-3** are heavily disordered, we measured the three structures at 123 K to check whether an order-disorder phase transition occurs at lower temperature (Tables S5-S8). The results demonstrate that all three structures remain almost unchanged upon cooling to 123 K with only tiny modification of their structural parameters. Nevertheless, a careful analysis of the structures reveals that the shapes of the atomic ellipsoids of the disordered atoms exhibit visible changes on cooling, indicating a temperature dependent dynamic motion of these atoms.

Table S9 shows the anisotropic parameters of the disordered atoms in **1**, e.g. the U11, U22 and U33 tensors which correspond to fluctuations along the *a*-, *b*- and *c*-axis, respectively.[42] At room temperature, the tensor values for the C1 atom are 0.030, 0.022 and 0.022 Å^2, indicating an isotropic behavior. For C4 to C8 atoms of the phenyl group, the U11 values are 3-4 times U22 or U33 suggesting a strong anisotropic fluctuation along the *a*-axis. For C2 and C3, the values are U11 ≈ U33 > U22. Similar situation is found for the polar Me-O group. The tensor values follow the sequence of U11 >> U33 > U22 for the C11, C12 and O3 atoms. These results suggest that the phenyl and Me-O groups in compound **1** can fluctuate in the *ac* plane at room temperature (Figure 1a).

When the temperature is lowed to 123 K, the U11 tensor values for the atoms C4 to C8, C11, C12 and O3 decrease significantly, associated with the increase of the corresponding U22 values. Obviously, the dynamic motions of these atoms are hampered at low temperature.

For compound **2**, the tensor values of the disordered atoms of the benzyl group (C1 to C7) at 296 K follow the sequence of U11 >> U22 ≈ U33 (Table S10), which is consistent with the pendulum-like movements of the benzyl groups in **2**. For the atoms of the Me-O group (C8 and O3), the tensor values follow the order U11 >> U33 > U22. Hence the fluctuation of the Me-O group is speculated to occur in the *ac* plane (Figure 1d). At 123 K, the U11 values of the disordered atoms become much smaller, resulting in parameters U11 ≈ U22 ≈ U33. The nearly isotropic behavior suggests the blocking of the motion at low temperature.

In the case of compound **3**, the tensor values of the disordered atoms at 296 K follow the sequence of U11 ≈ U33 > U22 (Table S11). However, the difference between the U11 (or U33) and U22 values is much smaller than those in **1** and **2**, indicating a slight fluctuation of the atoms in the *ac* plane. At 123 K, the values of the tensors decrease (U11 < U22 ≈ U33), revealing the blocking of fluctuation.

Dielectric properties

The comparison of anisotropic parameters for structures **1-3** at 296 and 123 K reveals the distinct fluctuation of the phenyl and Me-O groups in the ac plane in compounds **1** and **2**. The free rotation of the organic groups can be monitored using techniques such as solid state ^{2}H NMR,[21-26] neutron inelastic scattering,[43] Terahertz vibration,[44] and dielectric measurements.[27-30] The latter concerns with the reorientational motions of the dipolar groups.[45] For compounds **1-4**, although para-substituted phenyl groups are apolar, the Me-O and meta-substituted phenyl groups are polar. Therefore, dielectric relaxation properties are investigated to probe the influence of the substitutional position of the grafted Me-O groups on the ligand dynamics.

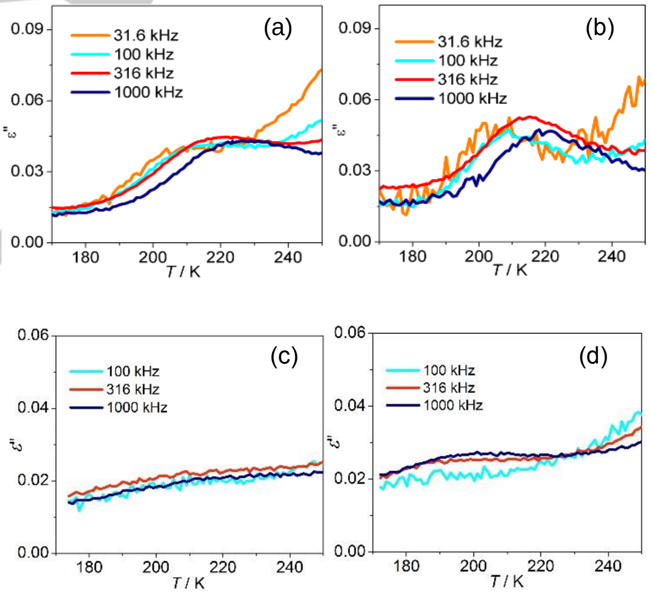

Figure 2. The ε'' *vs*. *T* plots at various frequencies for compounds **1** (a), **2** (b), **3** (c) and **4** (d).

The dielectric measurements were performed on compounds **1-4** using pressed plate samples in the frequency range of 31.6 - 1000 kHz and temperature range of 170 - 250 K. Figures 2a and 2b show the temperature dependent imaginary signals (ε'') of the dielectric constant for compounds **1** and **2**. At a fixed frequency (*f*), the curves show maximum at a certain temperature (ca. 200 – 220 K) in both cases. The maximum is related to the dipolar relaxation process in the samples, i.e., the rotation of the polar Me-O groups. When the frequency of the applied electric field is increased, the maximum of the peak shifts to a higher temperature. This kind of frequency dependent behavior indicates a thermally activated single relaxation process.[24] Thus the relaxation rate ($1/\tau$), characterizing the dielectric relaxation process, should follow the Arrhenius law (eq. 1),

$$\frac{1}{\tau} = \omega_0 \exp(\frac{-E_a}{k_B T}) \qquad (1)$$

where k_B corresponds to the Boltzmann's constant, T is the temperature, E_a is the activation energy for the relaxation process, and ω_0 is the pre-exponential factor. The ε" vs. T plots will reach a maximum when $\omega\tau = 1$, where ω is the angular frequency ($\omega = 2\pi f$). Thus, the frequency of the applied field can be used to estimate the relaxation rate at the temperature where ε" shows the maximum. The obtained E_a are 20.6 and 21.5 kcal/mol, and ω_0 are 3.8×10^{26} and 1.4×10^{28} s^{-1} for compounds **1** and **2**, respectively (Figure S7). The energy barriers are larger than those reported in the literature for the flip or rotational motion of the aromatic rings in different MOFs (4.0 – 15.1 kcal/mol),[20-26] which can be explained by the fact that the layer structures of **1** and **2** are more dense than those of MOFs. The latter often contains micro-pores to impart substantial free volume around the rotator ligands.

Notably, the E_a values for the two compounds are quite close to each other, but the ω_0 are significantly different by two orders of magnitude. The larger ω_0 in compound **2** suggests a faster dipolar relaxation process related to Me-O groups, which is attributed to their structural difference. In **2**, the (4-methoxybenzyl) phosphonate ligand has an additional $-CH_2-$ group comparing with the (4-methoxyphenyl)phosphonate ligand in **1**, which increases the flexibility and hence the rotation of the organic groups.

For compound **3**, the ε" value increases only slightly with increasing temperature (Figure 2c), in agreement with the centrosymmetric nature of the structure. Although compound **4** is polar, the ε" signals are much weaker than those observed in **1** and **2**. An unobtrusive maximum appears at ca. 200 K when the frequency reaches 1000 kHz (Figure 2d). The frequency dependence of the ε" signals is not evident below 250 K, attributed to the ordering arrangement of the organic groups in **4**.

Phase transitions in the dehydrated samples of compounds 3 and 4

Both the structural and dielectric measurements reveal that the dynamic motion of the Me-O groups can more easily occur in the para-substituted aromatic metal phosphonates of **1** and **2** than in the meta-substituted ones of **3** and **4**. This could be due to the larger steric hindrance in the meta-substituted compounds, providing less free volume proximate to the rotator. It is noticed that all of compounds **1-4** contain a coordination water molecule pointing out to the interlayer space. It forms hydrogen bonds with the phosphonate oxygen atoms within the inorganic layer, and also with the –CH- moieties from the phenyl or benzyl groups with the shortest C(H)···O distance being 3.550 Å for **1**, 7.287 Å for **2**, 3.347 Å for **3**, and 3.635 Å for **4**. The removal of the coordination water molecule could weaken the interactions between the organic groups and the layered inorganic backbone, and facilitate the fluctuation of the organic moieties.

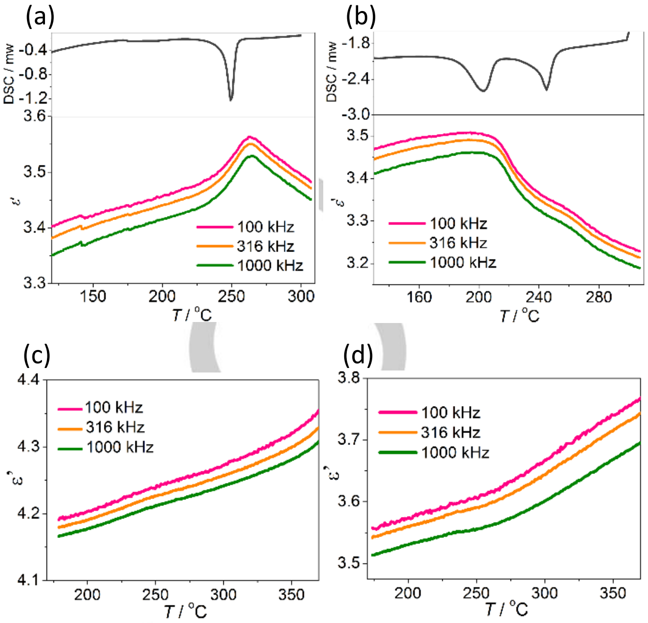

Figure 3. Temperature- and frequency-dependent dielectric constants together with the DSC diagrams in the heating process for compounds **3-de** (a) and **4-de** (b). Temperature- and frequency-dependent dielectric constants for compounds **3** (c) and **4** (d) are also presented as a comparison.

Thermal analyses were performed under nitrogen flow in the temperature range 30 – 500 °C (Figure S8). The weight losses between 128 and 174 °C are 6.7% for **1**, 6.6% for **2**, 7.0% for **3** and 6.2% for **4**, corresponding to the release of one water molecule (calcd. 6.8% for **1** and **3**, 6.5% for **2** and **4**). Above 174 °C, a wide plateau is observed until the compounds are decomposed at ca. 370 °C for **1** and ca. 410 °C for **2**-**4**. Remarkably, the simultaneously measured heat-flow curves (Figure S9) reveal an endothermic peak at 248 °C for **3**, and two endothermic peaks at 203 and 245 °C for **4**. On the contrary, no peak appears in the range 200 - 350 °C for **1** and **2**. It is evident that phase transitions occur in the dehydrated samples of **3** and **4** (abbreviated as **3-de** and **4-de**) above 200 °C, but not in those of **1** and **2** (abbreviated as **1-de** and **2-de**).

To further confirm the phase transition, DSC measurements were conducted for the four dehydrated samples obtained by heating the samples at 180 °C for one hour. No peak is observed for compounds **1-de** and **2-de** (Figure S10) and their PXRD patterns remaining the same between 180 and 300 °C (Figure S11), thus excluding any phase transitions in this temperature range for the two samples.

For compound **3-de**, the heating and cooling processes give a distinct endothermic peak at 251 °C and an exothermic peak at 229 °C, respectively (Figures 3 and S12). Clearly a phase transition occurs which is reversible upon heating and cooling. The phase transition can be monitored by the variable temperature PXRD measurements. As shown in Figure S13, the PXRD pattern of **3-de** (after heating **3** to 180 °C) is quite similar to that of the pristine compound **3**, indicating that the original layered structure is maintained after dehydration. However, when the temperature is increased to 220 °C, additional diffraction

10.1002/chem.201801301

peaks appear at 11.3° and 16.9°, the intensity of which increases with increasing temperature. In contrast, the peak intensities at 11.1 and 16.6° diminish and finally disappear at 280°, forming a new phase of the material. Unfortunately, we are not able to solve the crystal structure of this new phase because its single crystallinity cannot be maintained after dehydration and phase transition processes.

The DSC curve for compound **4-de** is more complicated (Figure S14). Two successive endothermic peaks are observed at 202 and 245 °C in the heating process, suggesting the presence of two-step phase transitions. This is confirmed by the variable temperature PXRD measurements (Figure S15). At 180 °C, the diffraction peak at 5.30° splits into two peaks at ca. 5.08° and 5.38°, indicating the coexistence of two phases. The intensity of the former increases with increasing temperature. This process should attribute to the first phase transition in compound **4-de**. When the temperature reaches 240 °C, the diffraction peak at 5.08° further splits into two peaks, corresponding to the second phase transition. Surprisingly, in the cooling process of the DSC measurement three exothermic peaks around 238, 195 and 138 °C are observed, suggesting three successive phase transitions upon cooling. The curve measured in the temperature range 100 - 220 °C shows a pair of peaks at 202 °C and 138 °C, indicating that the transition at 138 °C corresponds to the first transition at 202 °C in the heating mode.

In order to get insight into the origin of these phase transitions, dielectric relaxation spectroscopy was measured. The real component of the dielectric constant (ε') would show drastic changes when the phase transition arises from the motion and / or ordering of the polar groups. Indeed, both **3-de** and **4-de** show frequency-independent anomalies (Figures 3 and S16). The maxima are at ca. 263 °C for **3-de**, and 201 and 251°C for **4-de**, in agreement with the DSC and PXRD measurements upon heating. The results demonstrate that the motion of the polar phenyl and Me-O groups should be responsible to the phase transitions in compounds **3-de** and **4-de**.

Magnetic properties

The cobalt compounds are magnetically attractive due to the presence of strong spin-orbit coupling of the Co^{II} ion.[46] A number of cobalt phosphonates have been reported to show interesting magnetic behavior such as ferrimagnetism, weak ferromagnetism and metamagnetism.[47,48] Polar cobalt compounds can offer unique opportunities for exploring new multifunctional materials such as multiferroic materials combining polarity and magnetism.[49-51] Bearing this in mind, we also studied the magnetic properties of compounds **1-4**. Figures 4 and S17 show the temperature dependent magnetic susceptibilities measured under a dc field of 1 kOe and a temperature range of 1.9 - 300 K. At room temperature, the $\chi_m T$ products for compounds **1** - **4** are 3.08, 3.20, 3.38 and 3.31 $cm^3\ mol^{-1}$ K, respectively. These values are much larger than the spin-only value of 1.88 $cm^3\ mol^{-1}$ K for isolated Co^{II} ions (S = 3/2 and g = 2.0), attributed to the orbital contribution of the octahedral cobalt(II) ion. Upon cooling, the $\chi_m T$ values decrease continuously and approach to 0.10, 0.09, 0.13 and 0.10 $cm^3\ mol^{-1}$ K at 1.9 K for the four compounds, arising from antiferromagnetic (AF) interactions and / or spin-orbital couplings in the materials. The Weiss constants (θ) based on the Curie-Weiss fitting of the data above 80 K are -84.1, -46.7, -59.1 and -45.5 K for compounds **1-4**, respectively, indicating the propagation of moderate to strong AF interactions between the cobalt(II) centers.[46] In order to estimate the strength of AF interactions, one simple phenomenological eq. 2 can be used,[52]

$$\chi T = A\exp(-E_1/kT) + B\exp(-E_2/kT) \qquad (2)$$

where A+B equals the Curie constant (C), and E_1 and E_2 correspond to "activation energy" related to the spin-orbital coupling and to the AF interaction, respectively. As shown in Figure 4, all the experimental data of the present work are well fitted by this model. The obtained parameters are summarized in Table 3. The E_1/k values are consistent with those give in the literature for both the effects of spin-orbital coupling and site distortion (E_1/k of the order of 100 K).[53] For E_2/k, compounds **1** and **3** have similar values of 7.2 and 7.4 K, smaller than that for compounds **2** and **4** (8.6 and 8.1 K). This result suggests the strength of the AF coupling in the four compounds having the sequence of $J1 \approx J3 < J2 \approx J4$, consistent with the sequence for AF ordering temperatures (6.5, 10, 6 and 9 K based on the peak of χ_M *vs*. T plots) (Figure S17).

The magnetization (M) curves were measured at 1.9 K for the four compounds (Figure S19). In all cases, the magnetizations per Co increase almost linearly with increasing magnetic field and reach values of 0.74, 0.74, 0.90 and 0.80 $N\beta$ at 70 kOe for **1-4**, respectively. These values are much smaller than the saturation value of *ca*. 2.3 $N\beta$ for Co^{II} (S_{eff} = 1/2, g = 4.6). This difference is in line with the strong AF interaction as well as anisotropic effect in the compounds.[54]

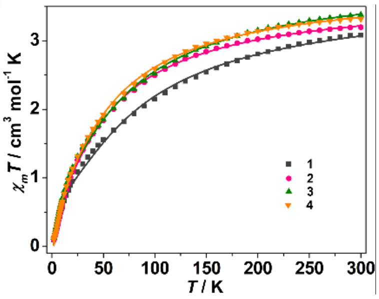

Figure 4. The $\chi_m T$ *vs*. T plots of the four compounds, solid lines are the best fit based on eq. 2.

Table 3. The obtained parameters based on eq. 2

Compound	A [$cm^3\ mol^{-1}$ K]	B [$cm^3\ mol^{-1}$ K]	-E_1/k [K]	-E_1/k [K]
1	2.46	1.28	-89.4	-7.2
2	2.20	1.50	-65.4	-8.6
3	2.42	1.56	-78.2	-7.4
4	2.30	1.52	-64.2	-8.1

Proper magneto-structural relationship should be built to explain the change of AF ordering temperature from compound to compound. Generally, the magnetic coupling mediated through O-P-O bridge is weak. In this case, the μ-O(P) bridges should play a key role for the mediation of magnetic interactions. Within the layer, the shortest Co⋯Co distances of the compounds are in the range of 3.70 - 3.82 Å (Table 2). The similar distances in

10.1002/chem.201801301

compounds **2** - **4** are not in accordance with their difference in AF ordering temperature. While the average Co-O-Co angles of compounds **1** and **3** are similar and 2^o smaller than the similar values of **2** and **4**. The strength of AF coupling can be dependent on the value of Co-O-Co angles, the larger values in compounds **2** and **4** will result in stronger AF interactions or higher AF ordering temperatures and *vice versa*.[55]

Conclusions

We report for the first time the dynamic motions of the organic groups in layered metal phosphonate systems. The structures of four cobalt phosphonate compounds Co(4-mopp)(H_2O) (**1**), Co(4-mobp)(H_2O) (**2**), Co(3-mopp)(H_2O) (**3**) and Co(3-mobp)(H_2O) (**4**), where 4- or 3-moppH_2 is (4- or 3-methoxyphenyl)phosphonic acid and 4- or 3-mobpH_2 is (4- or 3-methoxybenzyl)phosphonic acid, have been studied at 296 and 123 K. All bear similar layer topologies containing edge-sharing [Co_4O_4] rhombuses. Structural comparison of the anisotropic parameters obtained at 296 and 123 K indicates the fluctuation of the phenyl and Me-O groups in **1** and **2**. The motion of polar Me-O groups in the two compounds is further confirmed by dielectric measurements. Considering that compounds **1** and **2** differ from **3** and **4** by the substitution positions of the Me-O group (para- or meta-), the dynamic motion of the organic groups in metal aromatic phosphonates can be tuned by the positional isomerism of the ligand which cause different steric hindrance. Remarkably, the dehydrated compounds **3-de** and **4-de** show one- or two-step phase transitions above 200 ^oC, evidenced by both DSC and dielectric measurements. The phase transitions could be associated with the order-disorder or positional changes of the polar phenyl and methoxy groups. The work provides successful examples for the exploration of dynamic ligand motions in nonporous layered metal phosphonates.

Experimental Section

Materials and physical measurements: The reagents were obtained from commercial sources and used without further purification. Compound Co(3-mopp)(H_2O) (**3**) was synthesized according to the previously reported method.[39] Elemental analyses for C, H, N were performed on an Elementar Vario MICRO elemental analyzer. The infrared spectra were recorded on a Bruker Tensor 27 spectrometer with pressed KBr pellets in the 400 - 4000 cm^{-1} region. Thermogravimetric analyses were performed on a Mettler Toledo TGA/DSC 1 STAR^e instrument in the range of 30-500 ^oC under a nitrogen flow at a heating rate of 10 ^oC min^{-1}. Powder X-ray diffraction patterns (PXRD) were recorded on a Bruker ADVANCE D8 instrument using Cu-K_α radiation. The magnetic susceptibility data were obtained using polycrystalline samples by a Quantum Design MPMS SQUID VSM magnetometer. DSC curves were measured on a Mettler Toledo DSC823e instrument under a nitrogen flow at a heating rate of 10 ^oC min^{-1}. The temperature-dependent dielectric constants were measured using the two-probe AC impedance method at frequencies from 1 kHz to 1 MHz (Hewlett-Packard, HP4194A) using the temperature controller of a Linkam LTS-E350 system. The electrical contacts were prepared using gold paste (Tokuriki 8560) to attach the 25-μm ϕ gold wires to the 3-mm ϕ compressed pellet.

Synthesis of the phosphonate ligands. The ligands were synthesized through traditional Arbuzov reaction with or without the catalyst of $NiCl_2$. For (4- or 3-methoxyphenyl)phosphonic acid, 11 mmol triethyl phosphite was drop-wise added to a mixture of 10 mmol bromide and 1 mmol $NiCl_2$ in 100 mL three-necked bottle under the flow of N_2 at 150 ^oC during a period of ca. 0.5 hour. The mixture was further heated for 5 hours, and then cooled to room temperature. To the brown mixture was added 50 mL 1 mol/L HCl and the mixture was extracted by ethyl acetate (50 mL × 3). The organic layers were combined and dried by Na_2SO_4. Afterwards, the solvent was removed by distillation, and 20 mL concentrated HCl was added to the resulted oil, and the mixture was refluxed for 24 hours. Pale yellow solids were obtained after removing the solvent, which were washed by CH_3CN and dried in air resulting in a white solid. Yield: 63.2 % and 66.8 % for 4-moppH_2 and 3-moppH_2, respectively. Elemental anal. calcd. for $C_7H_9O_4P$: C, 44.69; H, 4.82 %. Found: C, 43.95; H, 4.87 % (for 4-moppH_2); C, 43.99; H, 4.89 % (for 3-moppH_2).

The (4- or 3-methoxybenzyl)phosphonic acid was synthesized based on similar route without $NiCl_2$ catalyst. Yield: 84.6 % and 89.0 % for 4-mobpH_2 and 3-mobpH_2, respectively. Elemental anal. calcd. for $C_8H_{11}O_4P$: C, 47.53; H, 5.48 %. Found: C, 47.20; H, 5.08 % (for 4-mobpH_2); C, 47.13; H, 5.67 % (for 3-mobpH_2).

Synthesis of Co(4-mopp)(H_2O) (1). $CoCl_2{\cdot}6H_2O$ (1.0 mmol, 234 mg) and 4-moppH_2 (0.5 mmol, 92 mg) were added to 4 mL distilled water and the pH value was adjusted to 3.8 - 4.0 with 0.5 M NaOH. Then the mixture was transferred to a 24 mL Teflon-lined autoclave and kept at 100 ^oC for two days. After cooling to room temperature, purple-red polycrystals were obtained and washed by distilled water. Yield: 16.5 mg (13 %, based on 4-moppH_2). The PXRD measurement confirmed the purity of the phase. Elemental anal. calcd. for $C_7H_9CoO_5P$: C, 31.96; H, 3.45. Found: C, 32.57; H, 3.79 %. IR (cm^{-1}): 3463(m), 3007(w), 1599(s), 1572(m), 1502(m), 1460(m), 1290(m), 1254(s), 1182(m), 1141(s), 1097(s), 1028(m), 964(s), 926(m), 696(m).

Synthesis of Co(4-mobp)(H_2O) (2). The procedure was similar to the synthesis of compound **1** except that 4-mobpH_2 was used instead of 4-moppH_2. Yield: 23.5 mg (17 %, based on 4-mobpH_2). Elemental anal. calcd. for $C_8H_{11}CoO_5P$: C, 34.68; H, 4.00. Found: C, 35.39; H, 4.30 %. IR (cm^{-1}): 3466(m), 2952(w), 1612(m), 1511(s), 1418(w), 1301(m), 1244(s), 1175(w), 1153(w), 1089(s), 1033(m), 961(s), 841(m), 820(w), 780(w), 704(w), 673(w).

Synthesis of Co(3-mobp)(H_2O) (4). $CoCl_2{\cdot}6H_2O$ (1.0 mmol, 234 mg) and 3-mobpH_2 (0.5 mmol, 92 mg) were added to 4 mL distilled water and the pH value was adjusted to 3.8 - 4.0 with 0.5 M NaOH. Then the mixture was transferred to a 24 mL Teflon-lined autoclave and kept at 100 ^oC for one day. After cooling to room temperature, purple-red polycrystals were obtained and washed by distilled water. Yield: 19.7 mg (14 %, based on 3-mobpH_2). Elemental anal. calcd. for $C_8H_{11}CoO_5P$: C, 34.68; H, 4.00. Found: C, 34.91; H, 4.00 %. IR (cm^{-1}): 3422(m), 2979(w), 1594(s), 1492(m), 1457(m), 1432(w), 1319(w), 1278(w), 1247(s), 1162(m), 1086(s), 1036(m), 961(s), 861(m), 796(m), 770(w), 737(w), 688(m).

Single-crystal structure determination. Single crystals of dimensions 0.5 × 0.05 × 0.05 mm^3 for **1**, 0.2 × 0.05 × 0.05 mm^3 for **2**, 0.05 × 0.04 × 0.03 mm^3 for **3** and 0.04 × 0.04 × 0.05 mm^3 for **4** were selected for indexing and intensity data collection on a Bruker APEX II CCD diffractometer using graphite-monochromatized Mo K_α radiation (λ = 0.71073 Å) at 296 K and 123 K. A hemisphere of data were collected using a narrow-frame method with scan widths of 0.30° in ω and an exposure time of 40 s/frame. The data were integrated using the Siemens SAINT program,[56] with the intensities corrected for Lorentz factor, polarization, air absorption, and absorption due to variation in the path length through the detector face plate. Absorption corrections were applied. The structures were solved by direct methods and refined on F^2 by full-matrix least-squares using SHELXTL.22.[57] All the non-hydrogen atoms were located from the Fourier maps, and were refined anisotropically. The disordered atoms in the compounds were refined anisotropically. The crystallographic data of the compounds are listed in Table 1 and S5. The selected bond lengths and angles are given in Tables S1-S4 and S6-S8.

Acknowledgements

Financial support by the National Natural Science Foundation of China (21731003) and the National Key R&D Program of China (2017YFA0303203) is acknowledged.

Keywords: Molecular motion • layer • cobalt phosphonate • dielectric • magnetic • polar

[1] C. S. Vogelsberg, M. A. Garcia-Garibay, *Chem. Soc. Rev.* **2012**, *41*, 1892–1910.

[2] P. H. Colberg, S. Y. Reigh, B. Robertson, R. Kapral, *Acc. Chem. Res.* **2014**, *47*, 3504 - 3511;

[3] M. G. L. van den Heuvel, C. Dekker, *Science* **2007**, *317*, 333 - 336.

[4] C. J. Bruns, J. F. Stoddart, *Acc. Chem. Res.* **2014**, *47*, 2186 - 2199.

[5] T. Akutagawa, H. Koshinaka, D. Sato, S. Takeda, S. Noro, H. Takahashi, R. Kumai, Y. Tokura, T. Nakamura, *Nat. Mater*. **2009**, *8*, 342 – 347.

[6] H. Kitagawa, Y. Kobori, M. Yamanaka, K. Yoza, K. Kobayashi, *Proc. Natl. Acad. Sci. USA* **2009**, *106*, 10444 - 10448;

[7] Q.-C. Zhang, F.-T. Wu, H.-M. Hao, H. Xu, H.-X. Zhao, L.-S. Long, R.-B. Huang, L.-S. Zheng, *Angew. Chem. Int. Ed*. **2013**, *52*, 12602 - 12605.

[8] W. Li, C.-T. He, Y. Zeng, C.-M. Ji, Z.-Y. Du, W.-X. Zhang, X.-M. Chen, *J. Am. Chem. Soc.* **2017**, 139, 8086−8089.

[9] S. Bracco, M. Beretta, A Cattaneo, A Comotti, A Falqui, K. Zhao, C. Rogers, P. Sozzani, *Angew. Chem. Int. Ed*. **2015**, *54*, 4773 - 4777.

[10] A. Comotti, S. Bracco, A. Yamamoto, M. Beretta, T. Hirukawa, N. Tohnai, M. Miyata, P. Sozzani, *J. Am. Chem. Soc.* **2014**, *136*, 618−621.

[11] J.-R. Li, R. J. Kuppler, H.-C. Zhou, *Chem. Soc. Rev*. **2009**, *38*, 1477 – 1450.

[12] H. Furukawa, U. Müller, O. M. Yaghi, *Angew. Chem. Int. Ed.* **2015**, *54*, 3417 – 3430.

[13] Z. Fang, B. Bueken, D. E. De Vos, R. A. Fischer, *Angew. Chem. Int. Ed*. **2015**, *54*, 7234 – 7254.

[14] M. L. Foo, R. Matsuda, S. Kitagawa, *Chem. Mater*. **2014**, *26*, 310 - 322.

[15] T. Zhang, W. Lin, *Chem. Soc. Rev.* **2014**, *43*, 5982 – 5993.

[16] J. Li, Q.-L. Zhu, Q. Xu, *Chem. Commun.* **2014**, *50*, 5899 - 5901.

[17] M. Yoon, K. Suh, S. Natarajan, K. Kim, *Angew. Chem. Int. Ed.* **2013**, *52*, 2688 – 2700.

[18] P. Ramaswamy, N. E. Wong, G. K. H. Shimizu, *Chem. Soc. Rev*. **2014**, *43*, 5913 - 5932.

[19] G. M. Espallargas, E. Coronado, *Chem. Soc. Rev.* **2018**, *47*, 533-557.

[20] A. Schneemann, V. Bon, I. Schwedler, I. Senkovska, S. Kaskel, R. A. Fischer, *Chem. Soc. Rev.* **2014**, *43*, 6062 - 6096.

[21] S. Horike, R. Matsuda, D. Tanaka, S. Matsubara, M. Mizuno, K. Endo, S. Kitagawa, *Angew. Chem. Int. Ed.* **2006**, *45*, 7226 – 7230.

[22] D. I. Kolokolov, H. Jobic, A. G. Stepanov, V. Guillerm, T. Devic, C. Serre, G. Férey, *Angew. Chem. Int. Ed*. **2010**, *49*, 4791 - 4794.

[23] S. L. Gould, D. Tranchemontagne, O. M. Yaghi, M. A. Garcia-Garibay, *J. Am. Chem. Soc*. **2008**, *130*, 3246 – 3247.

[24] S. Devautour-Vinot, G. Maurin, C. Serre, P. Horcajada, D. P. da Cunha, V. Guillerm, E. de S. Costa, F. Taulelle, C. Martineau, *Chem. Mater.* **2012**, *24*, 2168−2177.

[25] K. Zhu, V. N. Vukotic, C. A. O'Keefe, R. W. Schurko, S. J. Loeb, *J. Am. Chem. Soc.* **2014**, *136*, 7403−7409.

[26] C. S. Vogelsberg, F. J. Uribe-Romo, A. S. Lipton, S. Yang, K. N. Houk, S. Brown, M. A. Garcia-Garibay, *Proc. Natl. Acad. Sci. USA* **2017**, *114*, 13613–13618.

[27] W. Zhang, H.-Y. Ye, R. Graf, H. W. Spiess, Y.-F. Yao, R.-Q. Zhu, R.-G. Xiong, *J. Am. Chem. Soc.* **2013**, *135*, 5230−5233.

[28] W.-Y. Zhang, Y.-Y. Tang, P.-F. Li, P.-P. Shi, W.-Q. Liao, D.-W. Fu, H.-Y. Ye, Y. Zhang, R.-G. Xiong, *J. Am. Chem. Soc.* **2017**, *139*, 10897−10902.

[29] P. Jain, N. S. Dalal, B. H. Toby, H. W. Kroto, A. K. Cheetham, *J. Am. Chem. Soc*. **2008**, *130*, 10450 – 10451.

[30] G.-C. Xu, X.-M. Ma, L. Zhang, Z.-M. Wang, S. Gao, *J. Am. Chem. Soc*. **2010**, *132*, 9588 - 9890.

[31] G.-C. Xu, W. Zhang, X.-M. Ma, Y.-H. Chen, L. Zhang, H.-L. Cai, Z.-M. Wang, R.-G. Xiong, S. Gao, *J. Am. Chem. Soc*. **2011**, *133*, 14948 – 14951.

[32] P. Jain, V. Ramachandran, R. J. Clark, H. D. Zhou, B. H. Toby, N. S. Dalal, H. W. Kroto, A. K. Cheetham, *J. Am. Chem. Soc.* **2009**, *131*, 13625 – 13627.

[33] Y. Tian, S. Shen, J. Cong, L. Yan, S. Wang, Y. Sun, *J. Am. Chem. Soc*. **2016**, *138*, 782 - 785.

[34] B. Kundys, A. Lappas, M. Viret, V. Kapustianyk, V. Rudyk, S. Semak, C. Simon, I. Bakaimi, *Phys. Rev. B*, **2010**, *81*, 224434.

[35] A. O. Polyakov, A. H. Arkenbout, J. Baas, G. R. Blake, A. Meetsma, A. Caretta, P. H. M. Van Loosdrecht, T. T. M. Palstra, *Chem. Mater*. **2012**, *24*, 133 – 139.

[36] W.-Q. Liao, Y. Zhang, C.-L. Hu, J.-G. Mao, H.-Y. Ye, P.-F. Li, S. D. Huang, R.-G. Xiong, *Nat. Commun*. **2015**, *6*, 7338.

[37] A. Clearfield, K. Demadis, *Metal Phosphonate Chemistry: From Synthesis to Applications*, **2012**, Royal Society of Chemistry.

[38] S.-S. Bao, G. K. H. Shimizu, L.-M. Zheng, *Coord. Chem. Rev.* **2018**, DOI: 10.1016/j.ccr.2017.11.029

[39] Z.-S. Cai, Y. Shi, S.-S. Bao, Y. Shen, X.-H. Xia, L.-M. Zheng, *ACS Catal.* **2018**, *8*, 3895−3902.

[40] G. Cao, H. Lee, V. M. Lynch, T. E. Mallouk, *Inorg. Chem.* **1988**, *27*, 2781-2785.

[41] G. Cao, V. M. Lynch, L. N. Yacullo, *Chem. Mater.* **1993**, *5*, 1000-1006.

[42] M. Tadokoro, Y. Ohhata, Y. Shimazaki, S. Ishimaru, T. Yamada, Y. Nagao, T. Sugaya, K. Isoda, Y. Suzuki, H. Kitagawa, H. Matsui, *Chem. Eur. J.* **2014**, *20*, 13698 - 13709.

[43] D. I. Kolokolov, H. Jobic, A. Stepanov, M. Plazanet, M. Zbiri, J. Ollivier, V. Guillerm, T. Devic, C. Serre, G. Férey, *Eur. Phys. J. Special Topics* **2010**, *189*, 263.

[44] M. R. Ryder, B. Van de Voorde, B. Civalleri, T. D. Bennett, S. Mukhopadhyay, G. Cinque, F. Fernandez-Alonso, D. De Vos, S. Rudić, J.-C. Tan, *Phys. Rev. Lett.* **2017**, *118*, 255502.

[45] D. W. Fu, W. Zhang, H. L. Cai, Y. Zhang, J. Z. Ge, R. G. Xiong, S. D. Huang, *J. Am. Chem. Soc*. **2011**, *133*, 12780 - 12786;

[46] M. Kurmoo, *Chem. Soc. Rev*. **2009**, *38*, 1353 - 1379.

[47] S.-S. Bao, L.-M. Zheng, *Coord. Chem. Rev.* **2016**, *319*, 63–85.

[48] L.-R. Guo, S.-S. Bao, B. Liu, D. Zeng, J. Zhao, J. Du, L.-M. Zheng, *Chem. Eur. J.* **2012**, *18*, 9534 - 9542.

[49] G. Nénert, U. Adem, E. M. Bauer, C. Bellitto, G. Righini and T. T. M. Palstra, *Phys. Rev. B: Condens. Matter Mater. Phys.*, **2008**, *78*, 054443

[50] J. Huang, S.-S. Bao, L.-S. Ling, H. Zhu, Y.-Z. Li, L. Pi, L.-M. Zheng, *Chem. Eur. J.* **2012**, *18*, 10839 - 10842.

[51] X.-J. Yang, S.-S. Bao, M. Ren, N. Hoshino, T. Akutagawa, L.-M. Zheng, *Chem. Commun.* **2014**, *50*, 3979-3981.

[52] J.-M. Rueff, N. Masciocchi, P. Rabu, A. Sironi, A. Skoulios, *Chem. Eur. J.* **2002**, *8*, 1813 - 1820.

[53] R. L. Carlin, *Magnetochemistry*, Springer, Berlin, Heidelberg, **1986**.

[54] G. E. Kostakis, S. P. Perlepes, V. A. Blatov, D. M. Proserpio, A. K. Powell, *Coord. Chem. Rev*. **2012**, *256*, 1246 - 1278.

[55] J. B. Goodenough, *Magnetism and the Chemical Bond*, John Wiley & Sons, New York, London, **1963**.

[56] *SAINT, Program for Data Extraction and Reduction, Siemens Analytical X-ray Instruments*, Madison, WI, **1994** - **1996**.

[57] *SHELXTL (version 5.0), Reference Manual, Siemens Industrial Automation*, Analytical Instruments, Madison, WI, **1995**.

FULL PAPER

Layered metal phosphonates Co(4-mopp)(H_2O) (**1**), Co(4-mobp)(H_2O) (**2**), Co(3-mopp)(H_2O) (**3**) and Co(3-mobp)(H_2O) (**4**), where 4- or 3-moppH$_2$ is (4- or 3-methoxyphenyl)phosphonic acid and 4- or 3-mobpH$_2$ is (4- or 3-methoxybenzyl)phosphonic acid, are reported. The phenyl and Me-O groups rotate in **1** and **2** but not in **3** and **4**. The dehydrated compounds **3-de** and **4-de** show one- or two-step phase transitions above 200 ^oC.

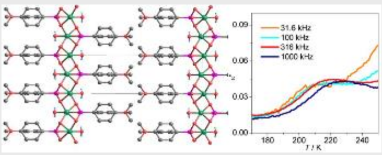

Zhong-Sheng Cai,[a] *Norihisa Hoshino,*[b] *Song-Song Bao,*[a] *Jiage Jia,*[a] *Tomoyuki Akutagawa,**[b] *and Li-Min Zheng**[a]

Page No. – Page No.

Dynamic Motion of Organic Ligands in Polar Layered Cobalt Phosphonates